IEEE Access
Multidisciplinary | Rapid Review | Open Access Journal

Received January 11, 2020, accepted February 14, 2020, date of publication February 18, 2020, date of current version February 27, 2020.

Digital Object Identifier 10.1109/ACCESS.2020.2974777

Analytical Method for Magnetic Field of Eccentric Magnetic Harmonic Gear

LIBING JING, (Member, IEEE), JUN GONG, AND TONG BEN
College of Electrical Engineering and New Energy, China Three Gorges University, Yichang 443002, China

Corresponding author: Libing Jing (jinglibing163@163.com)

This work was supported in part by the National Natural Science Foundation of China under Grant 51707072, in part by the China Postdoctoral Science Foundation under Grant 2018M632855, and in part by the Research Fund for Excellent Dissertation of China Three Gorges University under Grant 2020SSPY060.

ABSTRACT Eccentric magnetic harmonic gears (EMHG) can achieve high speed ratio transmission and large torque output by modulating the air gap length between permanent magnets (PM). The analytical method is based on the boundary perturbation method. The vector magnetic potential perturbation equation in the air gap region is established, and the general solution is obtained using the boundary conditions. According to the superposition principle, the air gap flux density of stator and rotor PMs acting alone is synthesized, and the electromagnetic torque and unbalanced magnetic pull are calculated. Last, we compare magnetic field distributions, electromagnetic torque and unbalanced magnetic pull computed by the analytical method with those obtained from finite-element method (FEM).

INDEX TERMS Eccentric magnetic harmonic gear, analytical method, magnetic field, electromagnetic torque, FEM.

I. INTRODUCTION

Compared with mechanical gears, magnetic gears (MG) can offer several advantages, namely, low noise, less friction, no lubrication, high reliability etc. MG is a device that transfers torque and speed by magnetic coupling instead of mechanical gear meshing. The torque density of concentric magnetic gear (CMG) can be up to 100kN·m/m^3 [1], [2]. In recent years, eccentric magnetic harmonic gear (EMHG) has been proposed, their torque density and transmission ratio are much larger than CMGs [3], [4]. It is particularly suitable for gear ratios higher than about 20:1, the transmitted torque is ripple free and torque density can be up to 150kN·m/m^3. Therefore, more and more scholars are paying attention to the EMHG.

Accurate calculation of air gap magnetic field is the key to optimum design of EMHG, whose structure is shown in Fig. 1. Because of the eccentric rotor revolution and rotation, the analysis of magnetic field will be more complicated. The calculation of air gap magnetic field includes finite element method (FEM) and analytical method. Although the FEM has high accuracy, it takes a long time and the mesh needs to be reconstructed when the rotor rotates. The analytical method has the advantages of fast calculation and clear physical concepts [5]–[9]. The free rotation of the rotor can be achieved without the constraint of meshing. Therefore, it is also suitable for calculating the magnetic field of magnetic gear with eccentric rotor. In the calculation and analysis of electromagnetic field, because of the complexity of boundary shape or medium characteristics in the analytical region, it is difficult to obtain exact analytical solution for the analytical calculation of air gap magnetic field, so it is necessary to adopt approximate analytical method.

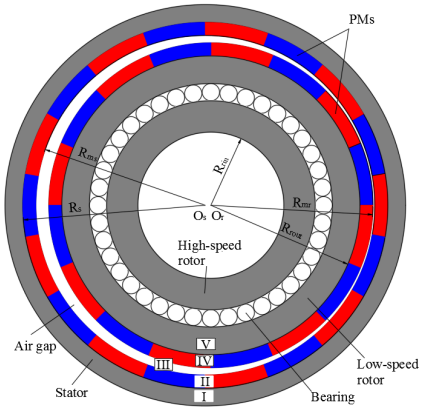

FIGURE 1. Geometry of the studied EMHG.

The associate editor coordinating the review of this manuscript and approving it for publication was Jenny Mahoney.

The boundary perturbation theory is used for the first time to analytically calculate the magnetic field of the rotor eccentricity of PM motor [10], [11]. In [12], Lubin proposed an analytical computation of the magnetic field distribution in a CMG, which is based on the resolution of Laplace's and Poisson's equations for each subdomain. The configuration and theoretical analysis of the CMG with Halbach PM Arrays has been discussed in [13], some parameters of CMG with Halbach PM Arrays have been optimized, and flux density and torque of CMG have been computed by an exact analytical method. Ref [14] analyzes and calculates the magnetic field and the electromagnetic torque of the CMG by adopting the exact analytical method, and optimizes the design of a CMG based on genetic algorithm toolbox of Matlab. In [15], Prof. Zhang proposed an analytical model of magnetic fields for magnetic harmonic gears, which is developed by the fractional linear transformation (FLT) method. In [16], the authors introduced new concept of complex relative air-gap permeance related to analytical field calculations in surface PM motors, which is developed from conformal transformation of the slot opening and used to accurately calculate the air-gap field for both radial and tangential components of the flux density in the slotted air gap. In [17], an analytical model is developed for the prediction of the air gap flux density in the eccentric permanent magnet inset machines at no-load and on-load conditions, which is fast and accurate.

In this paper, an analytical model of air gap magnetic field perturbation for EMHG is established. The eccentric perturbation ε in the analytical model is dimensionless. Firstly, when the PM on the low-speed rotor acts alone, according to the boundary conditions, the equation is solved in the rotor reference coordinate system, and the air gap flux density expression of the PM on the low-speed rotor can be obtained. Secondly, when the PM on the stator acts alone, the expression of the air gap flux density on the PM on the stator acts alone can be obtained in the stator reference coordinate system. Thirdly, according to the superposition principle, the air gap magnetic field of EMHG is synthesized and the electromagnetic torque and unbalanced magnetic pull are calculated. Finally, the analytical results are then verified with the finite-element method (FEM).

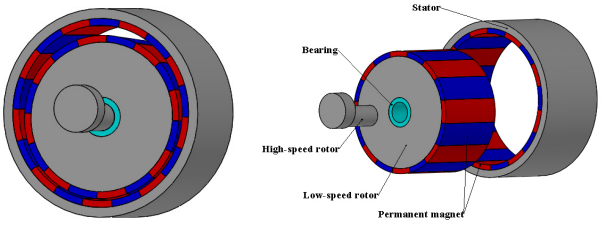

FIGURE 2. The EMHG with one sinusoidal cycle in the air-gap. (a) Construction of the EMHG, (b) Exploded view of (a).

II. ANALYTICAL MODEL

As shown in Fig. 2, the EMHG is composed of 3 parts, a high-speed inner rotor, a low-speed outer rotor and a stator.

The low-speed rotor is mounted on the high-speed rotor through the bearing, the high-speed rotor and low-speed rotor rotate eccentrically relative to the stator, and the motion paths are the same. There is a sinusoidal time-varying air gap length between the low-speed rotor and the stator. The magnetic field produced by two groups of PMs will be modulated, the pole pairs of the asynchronous space harmonics formed by one group of PMs is equal to that of the other group of PMs, so that the torque transmission and speed can be realized. In order to maximize the torque transfer ability of EMHG and according to the principle of magnetic field modulation, the polar pairs of stator permanent magnet should be equal to that of space harmonic magnetic field, the relationship between the polar pairs of the two parts is as follows,

$$p_s = p_r + 1 \tag{1}$$

where p_s and p_r are the number of pole pairs of stator and rotor, respectively. The gear ratio (G_r) is then given by,

$$G_r = -\frac{1}{P_r} \tag{2}$$

A. ANALYTICAL MODEL OF EMHG

For simplicity of analysis, the following assumptions are adopted:

1) The analytical field is a 2-D plane, and the end effects are neglected.

2) The demagnetization curve of the PM is linear with relative permeability $\mu_r = 1$.

3) The permeability of stator and rotor iron is infinite.

Fig. 1 shows the structure model of EMHG, which is divided into stator yoke subdomain I, stator PM subdomain II, air gap subdomain III, rotor PM subdomain IV and rotor yoke subdomain V. The meaning of each parameter is as follows: R_{rin} indicates the inner radius of the iron yoke of high-speed rotor; R_{rout} is the outer radius of the yoke of the low-speed rotor; R_{mr} represents the outer radius of PM of low speed rotor; R_{ms} is the inner radius of stator PM; R_s indicates the inner radius of stator iron yoke; O_r is the center of the rotor; O_s is the center of the stator.

Fig. 3 shows the analytical model of the EMHG. The analytical domain includes air gap subdomain III, stator PM subdomain II and rotor PM subdomain IV.

As shown in Fig. 3(a), when the low-speed rotor PMs act alone, the equivalent air gap domain includes air gap subdomain III and stator PM subdomain II. The *X*-*Y* coordinate system is established with the stator center O_s as the coordinate origin, any point P in the domain of the equivalent eccentric air gap can be represented by the r-θ cylindrical coordinate system with the rotor center O_r as the coordinate origin. The eccentricity distance between the rotor center and the stator center is a, and the eccentricity angle is φ. In Fig. 3(b), when the stator PMs act alone, the equivalent air gap domain includes the air gap subdomain III and the rotor

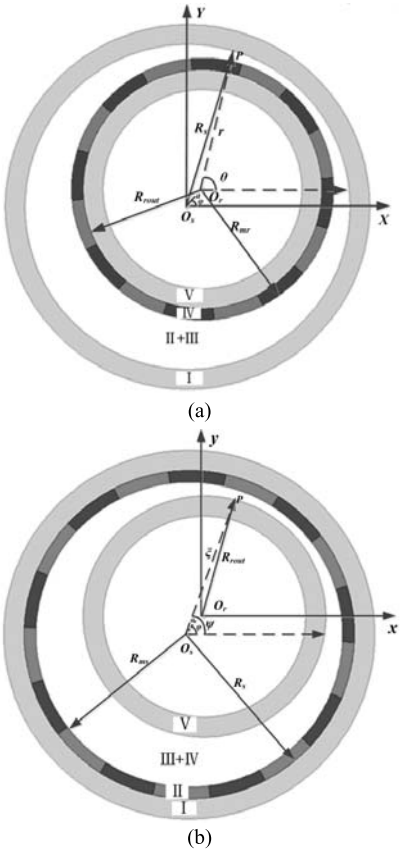

FIGURE 3. Analytical model of EMHG. (a) Rotor PM acts alone, (b) Stator PM acts alone.

PM subdomain IV. The *X*-*Y* coordinate system is established with the rotor center O_r as the coordinate origin, any point P in the equivalent eccentric air gap domain can be represented by ξ-ψ cylindrical coordinate system with the stator center O_s as the coordinate origin. The eccentricity distance between the rotor center and the stator center is a, and the eccentricity angle is φ.

B. PARTIAL DIFFERENTIAL EQUATIONS AND BOUNDARY CONDITIONS

When the low-speed rotor PMs act alone, from the geometric relationship [18], the equation of the inner circle track of the stator can be obtained as follows:

$$\begin{aligned} r &= \sqrt{R_s^2 - (a\sin(\theta-\phi))^2} - a\cos(\theta-\phi) \\ &\approx R_s - \frac{1}{2}\frac{a^2}{R_s}\sin^2(\theta-\phi) - a\cos(\theta-\phi) \end{aligned} \tag{3}$$

Let $r = R_s + \varepsilon\delta(\theta)$, let the eccentric disturbance $\varepsilon = \frac{a}{R_s}$, and it is dimensionless, so,

$$\begin{aligned} \delta(\theta) &= -\frac{1}{2}a\sin^2(\theta-\phi) - R_s\cos(\theta-\phi) \\ &= -\frac{1}{4}a + \frac{1}{4}a\cos 2(\theta-\phi) - R_s\cos(\theta-\phi) \end{aligned} \tag{4}$$

The stator boundary can be expressed as:

$$\begin{aligned} f(\theta) &= r - R_s - \varepsilon\delta(\theta) \\ &= r - R_s + \frac{1}{4}\varepsilon a - \frac{1}{4}\varepsilon a\cos 2(\theta-\phi) \\ &\quad + \varepsilon R_s\cos(\theta-\phi) = 0 \end{aligned} \tag{5}$$

The gradient solution of formula (5) can be obtained,

$$\begin{aligned} \nabla f(\theta) &= \frac{\partial f}{\partial r}e_r + \frac{1}{r}\frac{\partial f}{\partial \theta}e_\theta \\ &= e_r + \frac{\varepsilon}{r}[\frac{1}{2}a\sin 2(\theta-\phi) - R_s\sin(\theta-\phi)]e_\theta \end{aligned} \tag{6}$$

where e_r and e_θ are unit vectors in radial and tangential directions, respectively.

In order to obtain the normal vector at the inner radius of stator yoke, the module of formula 6 can be calculated,

$$n = \frac{\nabla f}{|\nabla f|} = e_r + \frac{\varepsilon}{r}[\frac{1}{2}a\sin 2(\theta-\phi) - R_s\sin(\theta-\phi)]e_\theta \tag{7}$$

The boundary condition of inner radius of stator yoke is as follows:

$$n \times (H_{r,i}e_r + H_{\theta,i}e_\theta) = 0 \tag{8}$$

where r and θ represent radial and tangential components, respectively. $i = 1$ and $i = 2$ are the analytical domain of air gap and PMs, respectively.

By substituting formula (7) with formula (8), the boundary conditions at the inner radius of stator yoke can be obtained,

$$\begin{aligned} H_{\theta,1}(r,\theta,\varepsilon) - \frac{\varepsilon}{r}[\frac{1}{2}a\sin 2(\theta-\phi) - R_s\sin(\theta-\phi)] \\ \cdot H_{r,1}(r,\theta,\varepsilon)\big|_{r=R_s+\varepsilon\delta(\theta)} = 0 \end{aligned} \tag{9}$$

The radial flux density at the outer radius of the rotor is zero, and its boundary condition is,

$$H_{\theta,2}(r,\theta,\varepsilon)\big|_{r=R_{rout}} = 0 \tag{10}$$

The radial and the tangential magnetic field strength at the interface of the PM surface are continuous, respectively. The boundary conditions at the interface are as follows:

$$B_{r,1}(r,\theta,\varepsilon)\big|_{r=R_{mr}} = B_{r,2}(r,\theta,\varepsilon)\big|_{r=R_{mr}} \tag{11}$$

$$H_{\theta,1}(r,\theta,\varepsilon)\big|_{r=R_{mr}} = H_{\theta,2}(r,\theta,\varepsilon)\big|_{r=R_{mr}} \tag{12}$$

According to perturbation theory, vector magnetic potential $\boldsymbol{A}$, magnetic flux density $\boldsymbol{B}$ and magnetic field intensity $\boldsymbol{H}$ can be expanded by power series of eccentric disturbance ε [19]

$$A_i = A_i^{(0)} + \varepsilon A_i^{(1)} + O(\varepsilon^2) \tag{13}$$

$$B_i = B_i^{(0)} + \varepsilon B_i^{(1)} + O(\varepsilon^2) \tag{14}$$

$$H_i = H_i^{(0)} + \varepsilon H_i^{(1)} + O(\varepsilon^2) \tag{15}$$

where $i = 1$ indicates the air gap domain, $i = 2$ indicates the PM domain.

In r-θ polar coordinate system, vector magnetic potential $\boldsymbol{A}$ satisfies Laplace equation and Poisson equation:

$$\begin{cases} \dfrac{\partial^2 A_1^{(j)}}{\partial r^2}+\dfrac{1}{r}\dfrac{\partial A_1^{(j)}}{\partial r}+\dfrac{1}{r^2}\dfrac{\partial^2 A_1^{(j)}}{\partial \theta^2}=0 \qquad j=0,1 \\ \dfrac{\partial^2 A_2^{(j)}}{\partial r^2}+\dfrac{1}{r}\dfrac{\partial A_2^{(j)}}{\partial r}+\dfrac{1}{r^2}\dfrac{\partial^2 A_2^{(j)}}{\partial \theta^2}=\begin{cases}-\dfrac{1}{\nu}\nabla\times M, & j=0\\ 0, & j=1\end{cases}\end{cases} \tag{16}$$

where v is the magnetoresistance, M is the magnetization of the PM, and its expression can be written,

$$M(r,\theta)=M_r(\theta)\overrightarrow{r}=\sum_{n=1,3,5\ldots}^{\infty} M_n\cos np(\theta-\theta_0)\overrightarrow{r} \tag{17}$$

where $M_n=\frac{2B_r}{\mu_0}\alpha_p\frac{\sin(n\pi\alpha_p/2)}{n\pi\alpha_p/2}$, B_r is the remanence of PM, μ_0 is the vacuum permeability, α_P is the polar arc coefficient, P is the number of poles of PM, θ_0 is the initial rotor deviation angle.

Equation (9) is expanded by Taylor series at $r=R_s$, and the boundary conditions of the zero order and the first order equations at the inner radius of stator yoke can be obtained,

$$\frac{\partial A_1^{(0)}(r,\theta)}{\partial r}\Big|_{r=R_s}=0 \tag{18}$$

$$\begin{aligned}&\frac{\partial A_1^{(1)}(r,\theta)}{\partial r}\Big|_{r=R_s}\\ &=-\frac{1}{R_s^2}[\frac{1}{2}a\sin 2(\theta-\phi)-R_s\sin(\theta-\phi)]\frac{\partial A_1^{(0)}(R_s,\theta)}{\partial\theta}\\ &\quad-[-\frac{1}{4}a+\frac{1}{4}a\cos 2(\theta-\phi)-R_s\cos(\theta-\phi)]\cdot\frac{\partial^2 A_1^{(0)}(R_s,\theta)}{\partial r^2}\end{aligned} \tag{19}$$

III. EXPRESSION OF AIR GAP FLUX DENSITY

A. MAGNETIC FIELD ANALYSIS

The boundary condition of the zero order equation of the eccentric air gap magnetic field is,

$$\begin{cases} \dfrac{\partial A_1^{(0)}(r,\theta)}{\partial r}\Big|_{r=R_\mathrm{s}}=0\\ -\dfrac{1}{\mu_0}\dfrac{\partial A_2^{(0)}(r,\theta)}{\partial r}\Big|_{r=R_\mathrm{rout}}=0\\ \dfrac{1}{r}\dfrac{\partial A_1^{(0)}(r,\theta)}{\partial\theta}\Big|_{r=R_{mr}}=\dfrac{1}{r}\dfrac{\partial A_2^{(0)}(r,\theta)}{\partial\theta}\Big|_{r=R_{mr}}\\ -\dfrac{1}{\mu_0}\dfrac{\partial A_1^{(0)}(r,\theta)}{\partial r}\Big|_{r=R_{mr}}=-\dfrac{1}{\mu_0}\dfrac{\partial A_2^{(0)}(r,\theta)}{\partial r}\Big|_{r=R_{mr}}\end{cases} \tag{20}$$

According to the boundary conditions, the equations (16) are solved. The analytical expressions of the zero order vector magnetic potential and the radial and tangential magnetic flux density in the air gap domain are as follows,

$$\begin{aligned}A_1^{(0)}(r,\theta)&=\sum_{n=1,3,5\ldots}^{\infty}[A_{1n}^{(0)}(r^{np_\mathrm{r}}+R_\mathrm{s}^{2np_\mathrm{r}}r^{-np_\mathrm{r}})\cos np_\mathrm{r}\theta\\ &\quad+C_{1n}^{(0)}(r^{np_\mathrm{r}}+R_\mathrm{s}^{2np_\mathrm{r}}r^{-np_\mathrm{r}})\sin np_\mathrm{r}\theta]\end{aligned} \tag{21}$$

$$\begin{aligned}&B_{r,1}^{(0)}(r,\theta)\\ &=\sum_{n=1,3,5\ldots}^{\infty}np_r[-A_{1n}^{(0)}(r^{np_r-1}+R_s^{2np_r}r^{-np_r-1})\sin np_r\theta\\ &\quad+C_{1n}^{(0)}(r^{np_r-1}+R_s^{2np_r}r^{-np_r-1})\cos np_r\theta]\end{aligned} \tag{22}$$

$$\begin{aligned}&B_{\theta,1}^{(0)}(r,\theta)\\ &=-\sum_{n=1,3,5\ldots}^{\infty}np_\mathrm{r}[A_{1n}^{(0)}(r^{np_\mathrm{r}-1}-R_\mathrm{s}^{2np_\mathrm{r}}r^{-np_\mathrm{r}-1})\cos np_\mathrm{r}\theta\\ &\quad+C_{1n}^{(0)}(r^{np_\mathrm{r}-1}-R_\mathrm{s}^{2np_\mathrm{r}}r^{-np_\mathrm{r}-1})\sin np_\mathrm{r}\theta]\end{aligned} \tag{23}$$

where $A_{1n}^{(0)}, B_{1n}^{(0)}, C_{1n}^{(0)}, D_{1n}^{(0)}$ are undetermined coefficients, see Appendix A for specific expressions.

The boundary condition of the first order equation of eccentric air gap magnetic field is,

$$\begin{cases} \dfrac{\partial A_1^{(1)}(r,\theta)}{\partial r}\Big|_{r=R_s}\\ =-\dfrac{1}{R_s^2}[\dfrac{1}{2}a\sin 2(\theta-\phi)-R_s\sin(\theta-\phi)]\dfrac{\partial A_1^{(0)}(r,\theta)}{\partial\theta}\Big|_{r=R_s}\\ -[-\dfrac{1}{4}a+\dfrac{1}{4}a\cos 2(\theta-\phi)-R_s\cos(\theta-\phi)]\dfrac{\partial^2 A_1^{(0)}(r,\theta)}{\partial r^2}\Big|_{r=R_s}\\ -\dfrac{1}{\mu_0}\dfrac{\partial A_2^{(1)}(r,\theta)}{\partial r}\Big|_{r=R_{rout}}=0\\ \dfrac{1}{r}\dfrac{\partial A_1^{(1)}(r,\theta)}{\partial\theta}\Big|_{r=R_{mr}}=\dfrac{1}{r}\dfrac{\partial A_2^{(1)}(r,\theta)}{\partial\theta}\Big|_{r=R_{mr}}\\ -\dfrac{1}{\mu_0}\dfrac{\partial A_1^{(1)}(r,\theta)}{\partial r}\Big|_{r=R_{mr}}=-\dfrac{1}{\mu_0}\dfrac{\partial A_2^{(1)}(r,\theta)}{\partial r}\Big|_{r=R_{mr}}\end{cases} \tag{24}$$

Similarly, the expression of the first order vector magnetic potential in the air gap domain is as follows,

$$\begin{aligned}A_1^{(1)}(r,\theta)=\sum_{n=1,3,5\ldots}^{\infty}&[(M_{1n}^{(1)}r^{np_\mathrm{r}}+N_{1n}^{(1)}r^{-np_\mathrm{r}})\cos np_\mathrm{r}\theta\\ &+(P_{1n}^{(1)}r^{np_\mathrm{r}}+Q_{1n}^{(1)}r^{-np_\mathrm{r}})\sin np_\mathrm{r}\theta\\ &+(A_{1n}^{(1)}r^{np_\mathrm{r}-1}+B_{1n}^{(1)}r^{-(np_\mathrm{r}-1)})\cos(np_\mathrm{r}-1)\theta\\ &+(C_{1n}^{(1)}r^{np_\mathrm{r}-1}+D_{1n}^{(1)}r^{-(np_\mathrm{r}-1)})\sin(np_\mathrm{r}-1)\theta\\ &+(E_{1n}^{(1)}r^{np_\mathrm{r}+1}+F_{1n}^{(1)}r^{-(np_\mathrm{r}+1)})\cos(np_\mathrm{r}+1)\theta\\ &+(G_{1n}^{(1)}r^{np_\mathrm{r}+1}+H_{1n}^{(1)}r^{-(np_\mathrm{r}+1)})\sin(np_\mathrm{r}+1)\theta\\ &+(S_{1n}^{(1)}r^{np_\mathrm{r}-2}+T_{1n}^{(1)}r^{-(np_\mathrm{r}-2)})\cos(np_\mathrm{r}-2)\theta\\ &+(U_{1n}^{(1)}r^{np_\mathrm{r}-2}+V_{1n}^{(1)}r^{-(np_\mathrm{r}-2)})\sin(np_\mathrm{r}-2)\theta\\ &+(W_{1n}^{(1)}r^{np_\mathrm{r}+2}+X_{1n}^{(1)}r^{-(np_\mathrm{r}+2)})\cos(np_\mathrm{r}+2)\theta\\ &+(Y_{1n}^{(1)}r^{np_\mathrm{r}+2}+Z_{1n}^{(1)}r^{-(np_\mathrm{r}+2)})\sin(np_\mathrm{r}+2)\theta]\end{aligned} \tag{25}$$

where $M_{1n}^{(1)}, N_{1n}^{(1)}, P_{1n}^{(1)}, Q_{1n}^{(1)}, A_{1n}^{(1)}, B_{1n}^{(1)}, C_{1n}^{(1)}, D_{1n}^{(1)}, E_{1n}^{(1)}, F_{1n}^{(1)}, G_{1n}^{(1)}, H_{1n}^{(1)}, S_{1n}^{(1)}, T_{1n}^{(1)}, U_{1n}^{(1)}, V_{1n}^{(1)}, W_{1n}^{(1)}, X_{1n}^{(1)}, Y_{1n}^{(1)}$, and $Z_{1n}^{(1)}$ are undetermined coefficients, see Appendix A for specific expressions.

Therefore, the expressions of radial and tangential flux density in the first order air gap domain are as follows:

$$\begin{aligned}
&B_{r,1}^{(1)}(r,\theta)\\
&=\frac{1}{r}\frac{\partial A_1^{(1)}}{\partial\theta}\\
&=\sum_{n=1,3.5\ldots}^{\infty}[-np_{\mathrm{r}}(M_{1n}^{(1)}r^{np_{\mathrm{r}}-1}+N_{1n}^{(1)}r^{-np_{\mathrm{r}}-1})\sin np_{\mathrm{r}}\theta\\
&\quad+np_{\mathrm{r}}(P_{1n}^{(1)}r^{np_{\mathrm{r}}-1}+Q_{1n}^{(1)}r^{-np_{\mathrm{r}}-1})\cos np_{\mathrm{r}}\theta\\
&\quad-(np_{\mathrm{r}}-1)(A_{1n}^{(1)}r^{np_{\mathrm{r}}-2}+B_{1n}^{(1)}r^{-np_{\mathrm{r}}})\sin(np_{\mathrm{r}}-1)\theta\\
&\quad+(np_{\mathrm{r}}-1)(C_{1n}^{(1)}r^{np_{\mathrm{r}}-2}+D_{1n}^{(1)}r^{-np_{\mathrm{r}}})\cos(np_{\mathrm{r}}-1)\theta\\
&\quad-(np_{\mathrm{r}}+1)(E_{1n}^{(1)}r^{np_{\mathrm{r}}}+F_{1n}^{(1)}r^{-np_r-2})\sin(np_r+1)\theta\\
&\quad+(np_r+1)(G_{1n}^{(1)}r^{np_r}+H_{1n}^{(1)}r^{-np_r-2})\cos(np_r+1)\theta\\
&\quad-(np_r-2)(S_{1n}^{(1)}r^{np_r-3}+T_{1n}^{(1)}r^{-np_r+1})\sin(np_r-2)\theta\\
&\quad+(np_r-2)(U_{1n}^{(1)}r^{np_r-3}+V_{1n}^{(1)}r^{-np_r+1})\cos(np_r-2)\theta\\
&\quad-(np_r+2)(W_{1n}^{(1)}r^{np_r+1}+X_{1n}^{(1)}r^{-np_r-3})\sin(np_r+2)\theta\\
&\quad+(np_r+2)(Y_{1n}^{(1)}r^{np_r+1}+Z_{1n}^{(1)}r^{-np_r-3})\cos(np_r+2)\theta]
\end{aligned}\tag{26}$$

$$\begin{aligned}
&B_{\theta,1}^{(1)}(r,\theta)\\
&=-\frac{\partial A_1^{(1)}}{\partial r}\\
&=-\sum_{n=1,3,5\ldots}^{\infty}[np_{\mathrm{r}}(M_{1n}^{(1)}r^{np_{\mathrm{r}}-1}-N_{1n}^{(1)}r^{-np_{\mathrm{r}}-1})\cos np_{\mathrm{r}}\theta\\
&\quad+np_{\mathrm{r}}(P_{1n}^{(1)}r^{np_{\mathrm{r}}-1}-Q_{1n}^{(1)}r^{-np_{\mathrm{r}}-1})\sin np_{\mathrm{r}}\theta\\
&\quad+(np_{\mathrm{r}}-1)(A_{1n}^{(1)}r^{np_r-2}-B_{1n}^{(1)}r^{-np_r})\cos(np_r-1)\theta\\
&\quad+(np_r-1)(C_{1n}^{(1)}r^{np_r-2}-D_{1n}^{(1)}r^{-np_r})\sin(np_r-1)\theta\\
&\quad+(np_r+1)(E_{1n}^{(1)}r^{np_r}-F_{1n}^{(1)}r^{-np_r-2})\cos(np_r+1)\theta\\
&\quad+(np_r+1)(G_{1n}^{(1)}r^{np_r}-H_{1n}^{(1)}r^{-np_r-2})\sin(np_r+1)\theta\\
&\quad+(np_r-2)(S_{1n}^{(1)}r^{np_r-3}-T_{1n}^{(1)}r^{-np_r+1})\cos(np_r-2)\theta\\
&\quad+(np_r-2)(U_{1n}^{(1)}r^{np_r-3}-V_{1n}^{(1)}r^{-np_r+1})\sin(np_r-2)\theta\\
&\quad+(np_r+2)(W_{1n}^{(1)}r^{np_r+1}-X_{1n}^{(1)}r^{-np_r-3})\cos(np_r+2)\theta\\
&\quad+(np_r+2)(Y_{1n}^{(1)}r^{np_r+1}-Z_{1n}^{(1)}r^{-np_r-3})\sin(np_r+2)\theta]
\end{aligned}\tag{27}$$

According to equation (14), we add the zero order air gap flux density and the first order air gap flux density, and eliminate the higher order infinitesimal of the eccentric disturbance ε. So the air gap flux density produced by the PM of the low speed rotor in the EMHG can be obtained,

$$\begin{aligned}
B_{r,1}&=B_{r,1}^{(0)}+\varepsilon B_{r,1}^{(1)}\\
B_{\theta,1}&=B_{\theta,1}^{(0)}+\varepsilon B_{\theta,1}^{(1)}
\end{aligned}\tag{28}$$

B. AIR GAP FLUX DENSITY PRODUCED BY STATOR PM

When the stator PM acts alone, the eccentric air gap magnetic field can also be obtained similarly. Set the pole pairs of the PMs to p_s. The eccentricity angle is φ, and the eccentricity disturbance $\varepsilon=a/R_{rout}$. The radial flux density $B_{\xi,1}$ and the tangential flux density $B_{\psi,1}$ produced by the stator PM acting alone are as follows,

$$\begin{aligned}
&B_{\xi,1}(\xi,\psi)\\
&=\sum_{n=1,3,5\ldots}^{\infty}np_s[-A_{2n}^{(0)}(\xi^{np_{\mathrm{s}}-1}+R_{rout}^{2np_{\mathrm{s}}}\xi^{-np_{\mathrm{s}}-1})\sin np_{\mathrm{s}}\psi\\
&\quad+C_{2n}^{(0)}(\xi^{np_{\mathrm{s}}-1}+R_{rout}^{2np_{\mathrm{s}}}\xi^{-np_{\mathrm{s}}-1})\cos np_{\mathrm{s}}\psi]\\
&\quad+\varepsilon\sum_{n=1,3,5\ldots}^{\infty}[-np_{\mathrm{s}}(M_{2n}^{(1)}\xi^{np_{\mathrm{s}}-1}+N_{2n}^{(1)}\xi^{-np_{\mathrm{s}}-1})\sin np_{\mathrm{s}}\psi\\
&\quad+np_{\mathrm{s}}(P_{2n}^{(1)}\xi^{np_{\mathrm{s}}-1}+Q_{2n}^{(1)}\xi^{-np_{\mathrm{s}}-1})\cos np_{\mathrm{s}}\psi\\
&\quad-(np_{\mathrm{s}}-1)(A_{2n}^{(1)}\xi^{np_{\mathrm{s}}-2}+B_{2n}^{(1)}\xi^{-np_{\mathrm{s}}})\sin(np_{\mathrm{s}}-1)\psi\\
&\quad+(np_{\mathrm{s}}-1)(C_{2n}^{(1)}\xi^{np_{\mathrm{s}}-2}+D_{2n}^{(1)}\xi^{-np_{\mathrm{s}}})\cos(np_{\mathrm{s}}-1)\psi\\
&\quad-(np_{\mathrm{s}}+1)(E_{2n}^{(1)}\xi^{np_{\mathrm{s}}}+F_{2n}^{(1)}\xi^{-np_{\mathrm{s}}-2})\sin(np_{\mathrm{s}}+1)\psi\\
&\quad+(np_{\mathrm{s}}+1)(G_{2n}^{(1)}\xi^{np_{\mathrm{s}}}+H_{2n}^{(1)}\xi^{-np_{\mathrm{s}}-2})\cos(np_{\mathrm{s}}+1)\psi\\
&\quad-(np_{\mathrm{s}}-2)(S_{2n}^{(1)}\xi^{np_{\mathrm{s}}-3}+T_{2n}^{(1)}\xi^{-np_{\mathrm{s}}+1})\sin(np_{\mathrm{s}}-2)\psi\\
&\quad+(np_{\mathrm{s}}-2)(U_{2n}^{(1)}\xi^{np_{\mathrm{s}}-3}+V_{2n}^{(1)}\xi^{-np_{\mathrm{s}}+1})\cos(np_{\mathrm{s}}-2)\psi\\
&\quad-(np_{\mathrm{s}}+2)(W_{2n}^{(1)}\xi^{np_{\mathrm{s}}+1}+X_{2n}^{(1)}\xi^{-np_{\mathrm{s}}-3})\sin(np_{\mathrm{s}}+2)\psi\\
&\quad+(np_{\mathrm{s}}+2)(Y_{2n}^{(1)}\xi^{np_{\mathrm{s}}+1}+Z_{2n}^{(1)}\xi^{-np_{\mathrm{s}}-3})\cos(np_{\mathrm{s}}+2)\psi]
\end{aligned}\tag{29}$$

$$\begin{aligned}
&B_{\psi,1}(\xi,\psi)\\
&=-\sum_{n=1,3,5\ldots}^{\infty}np_s[A_{2n}^{(0)}(\xi^{np_{\mathrm{s}}-1}-R_{rout}^{2np_{\mathrm{s}}}\xi^{-np_{\mathrm{s}}-1})\cos np_{\mathrm{s}}\psi\\
&\quad+C_{2n}^{(0)}(\xi^{np_{\mathrm{s}}-1}-R_{rout}^{2np_{\mathrm{s}}}\xi^{-np_{\mathrm{s}}-1})\sin np_{\mathrm{s}}\psi]\\
&\quad-\varepsilon\sum_{n=1,3,5\ldots}^{\infty}[np_{\mathrm{s}}(M_{2n}^{(1)}\xi^{np_{\mathrm{s}}-1}-N_{2n}^{(1)}\xi^{-np_{\mathrm{s}}-1})\cos np_{\mathrm{s}}\psi\\
&\quad+np_{\mathrm{s}}(P_{2n}^{(1)}\xi^{np_{\mathrm{s}}-1}-Q_{2n}^{(1)}\xi^{-np_{\mathrm{s}}-1})\sin np_{\mathrm{s}}\psi\\
&\quad+(np_{\mathrm{s}}-1)(A_{2n}^{(1)}\xi^{np_{\mathrm{s}}-2}-B_{2n}^{(1)}\xi^{-np_{\mathrm{s}}})\cos(np_{\mathrm{s}}-1)\psi\\
&\quad+(np_{\mathrm{s}}-1)(C_{2n}^{(1)}\xi^{np_{\mathrm{s}}-2}-D_{2n}^{(1)}\xi^{-np_{\mathrm{s}}})\sin(np_{\mathrm{s}}-1)\psi\\
&\quad+(np_{\mathrm{s}}+1)(E_{2n}^{(1)}\xi^{np_{\mathrm{s}}}-F_{2n}^{(1)}\xi^{-np_{\mathrm{s}}-2})\cos(np_{\mathrm{s}}+1)\psi\\
&\quad+(np_{\mathrm{s}}+1)(G_{2n}^{(1)}\xi^{np_{\mathrm{s}}}-H_{2n}^{(1)}\xi^{-np_{\mathrm{s}}-2})\sin(np_{\mathrm{s}}+1)\psi\\
&\quad+(np_{\mathrm{s}}-2)(S_{2n}^{(1)}\xi^{np_{\mathrm{s}}-3}-T_{2n}^{(1)}\xi^{-np_{\mathrm{s}}+1})\cos(np_{\mathrm{s}}-2)\psi\\
&\quad+(np_{\mathrm{s}}-2)(U_{2n}^{(1)}\xi^{np_{\mathrm{s}}-3}-V_{2n}^{(1)}\xi^{-np_{\mathrm{s}}+1})\sin(np_{\mathrm{s}}-2)\psi\\
&\quad+(np_{\mathrm{s}}+2)(W_{2n}^{(1)}\xi^{np_{\mathrm{s}}+1}-X_{2n}^{(1)}\xi^{-np_{\mathrm{s}}-3})\cos(np_{\mathrm{s}}+2)\psi\\
&\quad+(np_{\mathrm{s}}+2)(Y_{2n}^{(1)}\xi^{np_{\mathrm{s}}+1}-Z_{2n}^{(1)}\xi^{-np_{\mathrm{s}}-3})\sin(np_{\mathrm{s}}+2)\psi]
\end{aligned}\tag{30}$$

where $A_{2n}^{(0)}, B_{2n}^{(0)}, C_{2n}^{(0)}, D_{2n}^{(0)}, M_{2n}^{(1)}, N_{2n}^{(1)}, P_{2n}^{(1)}, Q_{2n}^{(1)}, A_{2n}^{(1)}, B_{2n}^{(1)}, C_{2n}^{(1)}, D_{2n}^{(1)}, E_{2n}^{(1)}, F_{2n}^{(1)}, G_{2n}^{(1)}, H_{2n}^{(1)}, S_{2n}^{(1)}, T_{2n}^{(1)}, U_{2n}^{(1)}, V_{2n}^{(1)}, W_{2n}^{(1)}, X_{2n}^{(1)}, Y_{2n}^{(1)}, Z_{2n}^{(1)}$ are undetermined coefficients, see Appendix B for specific expressions.

C. COMPOSITE AIR GAP FLUX DENSITY OF EMHG

By superposition of the air gap flux density when the stator PMs act alone and the air gap flux density when the rotor PMs acts alone, the superposition of flux density is shown in Fig. 4.

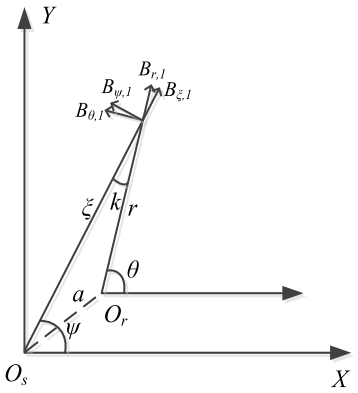

FIGURE 4. Superposition of flux density.

The radial and tangential air gap flux density expressions B_r and B_θ of the EMHG are obtained as follows,

$$\begin{aligned} B_r &= B_{r,1} + B_{\xi,1}\cos k + B_{\psi,1}\sin k \\ B_\theta &= B_{\theta,1} + B_{\psi,1}\cos k - B_{\xi,1}\sin k \end{aligned} \tag{31}$$

where $k = \theta - \psi$.

D. UNBALANCED MAGNETIC PULL AND ELECTROMAGNETIC TORQUE

According to the Maxwell stress tensor method, the unbalanced magnetic pull in the x-axis and y-axis direction can be obtained by integrating along the circular path through coordinate transformation.

$$\begin{aligned} F_x &= \int_0^{L_{ef}} \int_0^{2\pi} f_x r d\theta dz \\ &= L_{ef} r \int_0^{2\pi} [\frac{1}{2\mu_0}(B_r^2 - B_\theta^2)\cos\theta - \frac{1}{\mu_0}(B_r B_\theta)\sin\theta] d\theta \end{aligned} \tag{32}$$

$$\begin{aligned} F_y &= \int_0^{L_{ef}} \int_0^{2\pi} f_y r d\theta dz \\ &= L_{ef} r \int_0^{2\pi} [\frac{1}{2\mu_0}(B_r^2 - B_\theta^2)\sin\theta + \frac{1}{\mu_0}(B_r B_\theta)\cos\theta] d\theta \end{aligned} \tag{33}$$

The expression of electromagnetic torque is,

$$T = \frac{L_{ef} r^2}{\mu_0} \int_0^{2\pi} (B_r B_\theta) d\theta \tag{34}$$

where L_{ef} is the axial length of EMHG.

IV. APPLICATION EXAMPLE

In order to verify the correctness of the analytical model, an EMHG with a transmission ratio of 8:1 is used for the finite element modeling in this paper. In this study, when the eccentricity is about 0.57, $\varphi = 0$, the magnetic density at the radius $r = R_{mr} +$ (g-a)/2 is studied with the center of the low-speed rotor as the center. Table 1 lists the specific parameters of the EMHG.

TABLE 1. Parameters of EMHG.

Symbol	Quantity	Value
p_r	Pole pairs of rotor PM	8
p_s	Pole pairs of stator PM	9
R_{rout}	Outer radius of low speed rotor yoke	38mm
R_{mr}	Outer radius of PM for low speed rotor	42mm
R_{ms}	Inner radius of stator PM	45.5mm
R_s	Inner radius of stator yoke	49.5mm
h_{mr}	Thickness of rotor PM	4mm
h_{ms}	Thickness of stator PM	4mm
α_p	Pole arc coefficient	1
L_{ef}	Axial length	20mm
g	Average air gap length	3.5mm
g_{min}	Minimum air gap length	1.5mm
g_{max}	Maximum air gap length	5.5mm
B_r	PM remanence	1.25T
a	Eccentricity	2mm

A. AIR GAP MAGNETIC DENSITY AND HARMONIC ANALYSIS

Fig. 5 shows the distribution of magnetic flux lines in the air gap domain of the EMHG.

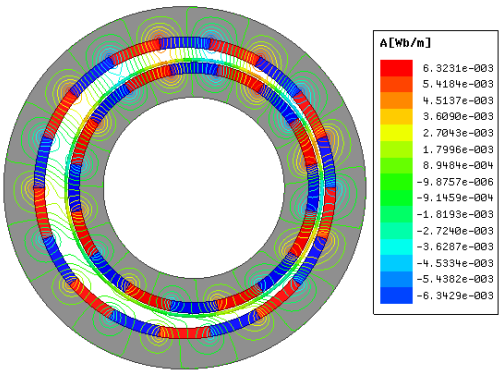

FIGURE 5. Magnetic flux lines.

Fig. 6 shows the radial and tangential components of the magnetic field in the air gap of the EMHG. It can be seen that the analytical results of the magnetic density in the radial and tangential air gap are in good agreement with the results of the FEM.

Fig. 7 shows the harmonic number of radial air gap flux density. It is obvious that the harmonic amplitude corresponding to the 8^{th} harmonic is the largest, which corresponds to the pole pairs of the rotor PM, and the harmonic amplitude corresponding to the 9^{th} harmonic is the second, which corresponds to the pole pairs of the stator PM. In order to achieve the maximum torque transmission of the EMHG, the pole pairs of the stator PM should meet $P_s = P_r + 1$.

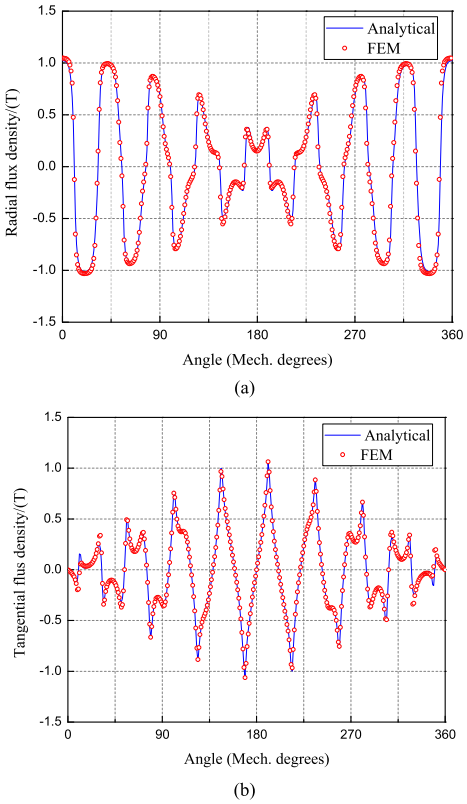

FIGURE 6. Flux density distribution in the air gap. (a) Radial component, (b) Tangential component.

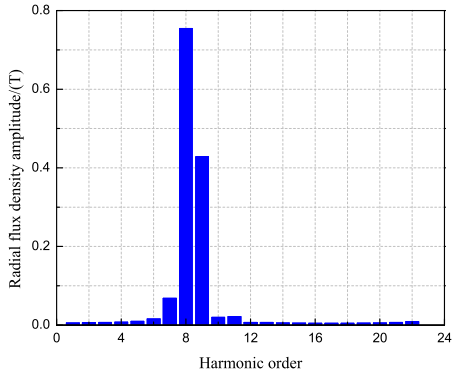

FIGURE 7. Harmonic spectrum.

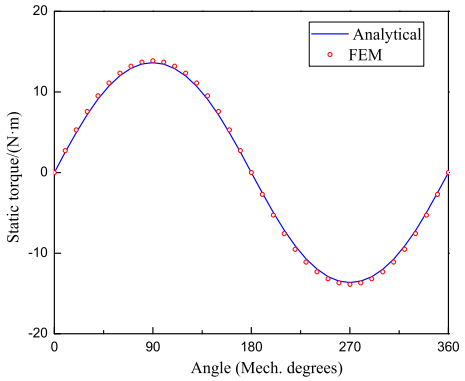

FIGURE 8. Static torque exerted on the low-speed rotor.

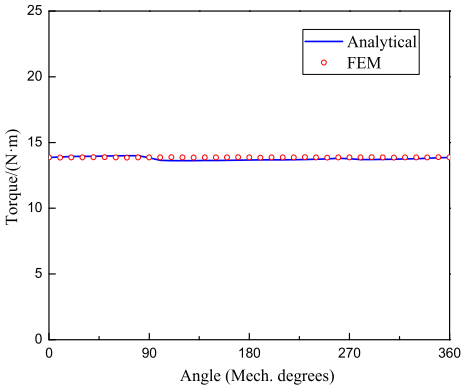

FIGURE 9. Output torque exerted on the low-speed rotor.

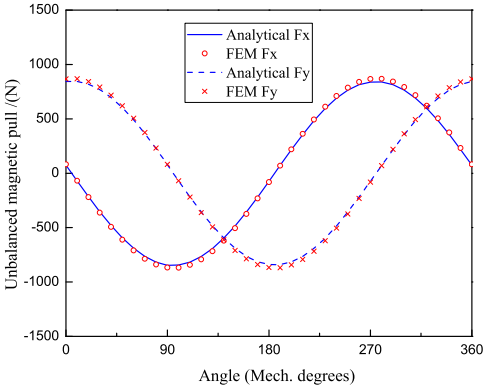

FIGURE 10. Unbalanced magnetic pull.

B. TORQUE AND UNBALANCED MAGNETIC PULL

Fig. 8 shows the static torque of the low speed rotor. In FEM, rotate the phase angle of the high-speed rotor from 0° to 360° and keep the position of the PM on the low-speed rotor unchanged. Calculate the electromagnetic torque every 10° interval, and a total of 37 electromagnetic torque values are obtained. The analytical solution of static torque is obtained by formula (34). As can be seen from Fig. 8, the results of analytical method are in good agreement with those of FEM.

Set the rotation angles of high-speed rotor and low-speed rotor, respectively. When the eccentricity angle of the high-speed rotor is changed from 0° to 360°, and the low-speed rotor rotates $(\varphi/8)°$ in the opposite direction to the high-speed rotor, the output constant electromagnetic torque of the low-speed rotor at various φ angles can be obtained. Fig. 9 shows the output constant torque of the low-speed rotor. The torque calculation result is 13.63N·m. It can be seen that the analytical results of the constant torque of the low-speed rotor are consistent with the wave trend of the FEM results.

Fig. 10 shows the curve of unbalanced magnetic pull F_x and F_y, which are the unbalanced magnetic pull of low-speed rotor along the x-axis and y-axis, respectively. As shown in Fig. 10, the analytical results of unbalanced magnetic pull are in good agreement with the results of FEM.

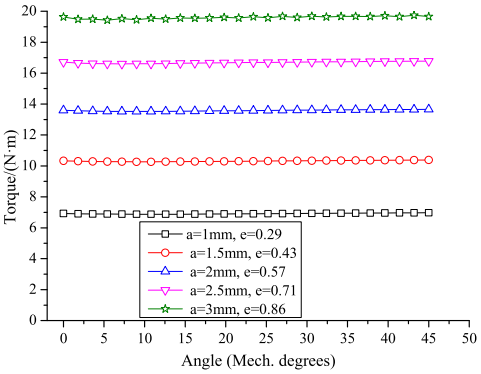

FIGURE 11. Variation of torque with different of eccentricity.

Fig. 11 shows the output torque of the low-speed rotor of the EMHG calculated by the analytical method under different eccentricity. As can be seen from that the torque value increases gradually with the increase of eccentricity. The torque ripple is very small in the transmitted torque.

Table 2 shows the calculation time of analytical method and FEM. It can be seen from the Table that the time of analytical method is much less than that of FEM.

TABLE 2. Comparison of analytical method and FEM.

Method	Analytical	FEM
CPU time(s)	1.49	101

V. CONCLUSION

In this paper, a perturbation analytical method is proposed to compute the distribution of the air gap magnetic field and the electromagnetic torque for EMHG. The expressions of air gap magnetic field are determined by solving two-dimensional Laplace equation and Poisson equation. The eccentric circle trajectory equation can accurately describe the boundary conditions of inner radius of stator and outer radius of rotor, which takes the eccentric disturbing momentum as the perturbation variable. The correctness of the analytical method is verified by comparing the results of the analytical method with those of the FEM. The physical concept of the analytical model is clear and the calculation is convenient, which provides an effective method for the magnetic field calculation and optimization design of the EMHG.

APPENDIXES

APPENDIX A

When the rotor PMs act alone, the expression of undetermined coefficient of the zero order equation, $A_{1n}^{(0)}, B_{1n}^{(0)}, C_{1n}^{(0)}, D_{1n}^{(0)}$ are:

$$A_{1n}^{(0)} = \frac{\mu_0 M_n \sin np_r\theta_0}{2[(np_r)^2-1](R_s^{2np_r}-R_{rout}^{2np_r})} \cdot \left[(1-np_r)R_{mr}^{np_r+1} + (np_r+1)R_{rout}^{2np_r}R_{mr}^{-np_r+1} - 2R_{rout}^{np_r+1}\right] \tag{A.1}$$

$$B_{1n}^{(0)} = \frac{\mu_0 M_n \sin np_r\theta_0 R_s^{2np_r}}{2[(np_r)^2-1](R_s^{2np_r}-R_{rout}^{2np_r})} \cdot \left[(1-np_r)R_{mr}^{np_r+1} + (np_r+1)R_{rout}^{2np_r}R_{mr}^{-np_r+1} - 2R_{rout}^{np_r+1}\right] \tag{A.2}$$

$$C_{1n}^{(0)} = \frac{\mu_0 M_n \cos np_r\theta_0}{2[(np_r)^2-1](R_s^{2np_r}-R_{rout}^{2np_r})} \cdot \left[(np_r-1)R_{mr}^{np_r+1} - (np_r+1)R_{rout}^{2np_r}R_{mr}^{-np_r+1} + 2R_{rout}^{np_r+1}\right] \tag{A.3}$$

$$D_{1n}^{(0)} = \frac{\mu_0 M_n R_s^{2np_r} \cos np_r\theta_0}{2[(np_r)^2-1](R_s^{2np_r}-R_{rout}^{2np_r})} \cdot \left[(np_r-1)R_{mr}^{np_r+1} - (np_r+1)R_{rout}^{2np_r}R_{mr}^{-np_r+1} + 2R_{rout}^{np_r+1}\right] \tag{A.4}$$

The expression of undetermined coefficient of the first order equation, $M_{1n}^{(1)}, N_{1n}^{(1)}, P_{1n}^{(1)}, Q_{1n}^{(1)}, A_{1n}^{(1)}, B_{1n}^{(1)}, C_{1n}^{(1)}, D_{1n}^{(1)}, E_{1n}^{(1)}, F_{1n}^{(1)}, G_{1n}^{(1)}, H_{1n}^{(1)}, S_{1n}^{(1)}, T_{1n}^{(1)}, U_{1n}^{(1)}, V_{1n}^{(1)}, W_{1n}^{(1)}, X_{1n}^{(1)}, Y_{1n}^{(1)}$, and $Z_{1n}^{(1)}$:

$$M_{1n}^{(1)} = \frac{\frac{1}{2}anp_r R_s^{2np_r-1}A_{1n}^{(0)}}{R_s^{2np_r}-R_{rout}^{2np_r}} \tag{A.5}$$

$$N_{1n}^{(1)} = \frac{\frac{1}{2}anp_r R_{rout}^{2np_r}R_s^{2np_r-1}A_{1n}^{(0)}}{R_s^{2np_r}-R_{rout}^{2np_r}} \tag{A.6}$$

$$P_{1n}^{(1)} = \frac{\frac{1}{2}anp_r R_s^{2np_r-1}C_{1n}^{(0)}}{R_s^{2np_r}-R_{rout}^{2np_r}} \tag{A.7}$$

$$Q_{1n}^{(1)} = \frac{\frac{1}{2}anp_r R_{rout}^{2np_r}R_s^{2np_r-1}C_{1n}^{(0)}}{R_s^{2np_r}-R_{rout}^{2np_r}} \tag{A.8}$$

$$A_{1n}^{(1)} = \frac{np_r R_s^{2np_r-1}(A_{1n}^{(0)}\cos\phi + C_{1n}^{(0)}\sin\phi)}{R_s^{2np_r-2}-R_{rout}^{2np_r-2}} \tag{A.9}$$

$$B_{1n}^{(1)} = \frac{np_r R_{rout}^{2np_r-2}R_s^{2np_r-1}(A_{1n}^{(0)}\cos\phi + C_{1n}^{(0)}\sin\phi)}{R_s^{2np_r-2}-R_{rout}^{2np_r-2}} \tag{A.10}$$

$$C_{1n}^{(1)} = \frac{np_r R_s^{2np_r-1}(-A_{1n}^{(0)}\sin\phi + C_{1n}^{(0)}\cos\phi)}{R_s^{2np_r-2}-R_{rout}^{2np_r-2}} \tag{A.11}$$

$$D_{1n}^{(1)} = \frac{np_r R_{rout}^{2np_r-2}R_s^{2np_r-1}(-A_{1n}^{(0)}\sin\phi + C_{1n}^{(0)}\cos\phi)}{R_s^{2np_r-2}-R_{rout}^{2np_r-2}} \tag{A.12}$$

$$E_{1n}^{(1)} = \frac{np_r R_s^{2np_r+1}(A_{1n}^{(0)}\cos\phi - C_{1n}^{(0)}\sin\phi)}{R_s^{2np_r+2}-R_{rout}^{2np_r+2}} \tag{A.13}$$

$$F_{1n}^{(1)} = \frac{np_r R_{rout}^{2np_r+2}R_s^{2np_r+1}(A_{1n}^{(0)}\cos\phi - C_{1n}^{(0)}\sin\phi)}{R_s^{2np_r+2}-R_{rout}^{2np_r+2}} \tag{A.14}$$

$$G_{1n}^{(1)} = \frac{np_r R_s^{2np_r+1}(A_{1n}^{(0)}\sin\phi + C_{1n}^{(0)}\cos\phi)}{R_s^{2np_r+2}-R_{rout}^{2np_r+2}} \tag{A.15}$$

$$H_{1n}^{(1)} = \frac{np_r R_r^{2np_r+2} R_s^{2np_r+1}(A_{1n}^{(0)}\sin\phi + C_{1n}^{(0)}\cos\phi)}{R_s^{2np_r+2} - R_{rout}^{2np_r+2}} \quad (A.16)$$

$$S_{1n}^{(1)} = \frac{-\frac{1}{4}anp_r R_s^{2np_r-3}(A_{1n}^{(0)}\cos 2\phi + C_{1n}^{(0)}\sin 2\phi)}{R_s^{2np_r-4} - R_{rout}^{2np_r-4}} \quad (A.17)$$

$$T_{1n}^{(1)} = \frac{-\frac{1}{4}anp_r R_{rout}^{2np_r-4} R_s^{2np_r-3}(A_{1n}^{(0)}\cos 2\phi + C_{1n}^{(0)}\sin 2\phi)}{R_s^{2np_r-4} - R_{rout}^{2np_r-4}} \quad (A.18)$$

$$U_{1n}^{(1)} = \frac{-\frac{1}{4}anp_r R_s^{2np_r-3}(-A_{1n}^{(0)}\sin 2\phi + C_{1n}^{(0)}\cos 2\phi)}{R_s^{2np_r-4} - R_{rout}^{2np_r-4}} \quad (A.19)$$

$$V_{1n}^{(1)} = \frac{-\frac{1}{4}anp_r R_{rout}^{2np_r-4} R_s^{2np_r-3}(-A_{1n}^{(0)}\sin 2\phi + C_{1n}^{(0)}\cos 2\phi)}{R_s^{2np_r-4} - R_{rout}^{2np_r-4}} \quad (A.20)$$

$$W_{2n}^{(1)} = \frac{-\frac{1}{4}anp_r R_s^{2np_r+1}(A_{1n}^{(0)}\cos 2\phi - C_{1n}^{(0)}\sin 2\phi)}{R_s^{2np_r+4} - R_{rout}^{2np_r+4}} \quad (A.21)$$

$$X_{1n}^{(1)} = \frac{-\frac{1}{4}anp_r R_{rout}^{2np_r+4} R_s^{2np_r+1}(A_{1n}^{(0)}\cos 2\phi - C_{1n}^{(0)}\sin 2\phi)}{R_s^{2np_r+4} - R_{rout}^{2np_r+4}} \quad (A.22)$$

$$Y_{1n}^{(1)} = \frac{-\frac{1}{4}anp_r R_s^{2np_r+1}(A_{1n}^{(0)}\sin 2\phi + C_{1n}^{(0)}\cos 2\phi)}{R_s^{2np_r+4} - R_{rout}^{2np_r+4}} \quad (A.23)$$

$$Z_{1n}^{(1)} = \frac{-\frac{1}{4}anp_r R_{rout}^{2np_r+4} R_s^{2np_r+1}(A_{1n}^{(0)}\sin 2\phi + C_{1n}^{(0)}\cos 2\phi)}{R_s^{2np_r+4} - R_{rout}^{2np_r+4}} \quad (A.24)$$

APPENDIX B

When the stator PMs act alone, the expression of undetermined coefficient of the zero order equation, $A_{2n}^{(0)}, B_{2n}^{(0)}, C_{2n}^{(0)}, D_{2n}^{(0)}$ are:

$$A_{2n}^{(0)} = \frac{\mu_0 M_n \sin np_s\psi_0}{2[(np_s)^2-1](R_{rout}^{2np_s} - R_s^{2np_s})} \cdot \left[(1-np_s)R_{ms}^{np_s+1} + (np_s+1)R_s^{2np_s}R_{ms}^{-np_s+1} - 2R_s^{np_s+1}\right] \quad (B.1)$$

$$B_{2n}^{(0)} = \frac{\mu_0 M_n \sin np_s\psi_0 R_{rout}^{2np_s}}{2[(np_s)^2-1](R_{rout}^{2np_s} - R_s^{2np_s})} \cdot \left[(1-np_s)R_{ms}^{np_s+1} + (np_s+1)R_s^{2np_s}R_{ms}^{-np_s+1} - 2R_s^{np_s+1}\right] \quad (B.2)$$

$$C_{2n}^{(0)} = \frac{\mu_0 M_n \cos np_s\psi_0}{2[(np_s)^2-1](R_{rout}^{2np_s} - R_s^{2np_s})} \cdot \left[(np_s-1)R_{ms}^{np_s+1} - (np_s+1)R_s^{2np_s}R_{ms}^{-np_s+1} + 2R_s^{np_s+1}\right] \quad (B.3)$$

$$D_{2n}^{(0)} = \frac{\mu_0 M_n R_{rout}^{2np_s} \cos np_s\psi_0}{2[(np_s)^2-1](R_{rout}^{2np_s} - R_s^{2np_s})} \cdot \left[(np_s-1)R_{ms}^{np_s+1} - (np_s+1)R_s^{2np_s}R_{ms}^{-np_s+1} + 2R_s^{np_s+1}\right] \quad (B.4)$$

The expression of undetermined coefficient of the first order equation, $A_{2n}^{(0)}, B_{2n}^{(0)}, C_{2n}^{(0)}, D_{2n}^{(0)}, M_{2n}^{(1)}, N_{2n}^{(1)}, P_{2n}^{(1)}, Q_{2n}^{(1)}, A_{2n}^{(1)}, B_{2n}^{(1)}, C_{2n}^{(1)}, D_{2n}^{(1)}, E_{2n}^{(1)}, F_{2n}^{(1)}, G_{2n}^{(1)}, H_{2n}^{(1)}, S_{2n}^{(1)}, T_{2n}^{(1)}, U_{2n}^{(1)}, V_{2n}^{(1)}, W_{2n}^{(1)}, X_{2n}^{(1)}, Y_{2n}^{(1)}, Z_{2n}^{(1)}$ are:

$$M_{2n}^{(1)} = \frac{\frac{1}{2}anp_s R_{rout}^{2np_s-1} A_{2n}^{(0)}}{R_{rout}^{2np_s} - R_s^{2np_s}} \quad (B.5)$$

$$N_{2n}^{(1)} = \frac{\frac{1}{2}anp_s R_s^{2np_s} R_{rout}^{2np_s-1} A_{2n}^{(0)}}{R_{rout}^{2np_s} - R_s^{2np_s}} \quad (B.6)$$

$$P_{2n}^{(1)} = \frac{\frac{1}{2}anp_s R_{rout}^{2np_s-1} C_{2n}^{(0)}}{R_{rout}^{2np_s} - R_s^{2np_s}} \quad (B.7)$$

$$Q_{2n}^{(1)} = \frac{\frac{1}{2}anp_s R_s^{2np_s} R_{rout}^{2np_s-1} C_{2n}^{(0)}}{R_{rout}^{2np_s} - R_s^{2np_s}} \quad (B.8)$$

$$A_{2n}^{(1)} = -\frac{np_s R_{rout}^{2np_s-1}(A_{2n}^{(0)}\cos\phi + C_{2n}^{(0)}\sin\phi)}{R_{rout}^{2np_s-2} - R_s^{2np_s-2}} \quad (B.9)$$

$$B_{2n}^{(1)} = -\frac{np_s R_s^{2np_s-2} R_{rout}^{2np_s-1}(A_{2n}^{(0)}\cos\phi + C_{2n}^{(0)}\sin\phi)}{R_{rout}^{2np_s-2} - R_s^{2np_s-2}} \quad (B.10)$$

$$C_{2n}^{(1)} = -\frac{np_s R_{rout}^{2np_s-1}(-A_{2n}^{(0)}\sin\phi + C_{2n}^{(0)}\cos\phi)}{R_{rout}^{2np_s-2} - R_s^{2np_s-2}} \quad (B.11)$$

$$D_{2n}^{(1)} = -\frac{np_s R_s^{2np_s-2} R_{rout}^{2np_s-1}(-A_{2n}^{(0)}\sin\phi + C_{2n}^{(0)}\cos\phi)}{R_{rout}^{2np_s-2} - R_s^{2np_s-2}} \quad (B.12)$$

$$E_{2n}^{(1)} = -\frac{np_s R_{rout}^{2np_s+1}(A_{2n}^{(0)}\cos\phi - C_{2n}^{(0)}\sin\phi)}{R_{rout}^{2np_s+2} - R_s^{2np_s+2}} \quad (B.13)$$

$$F_{2n}^{(1)} = -\frac{np_s R_s^{2np_s+2} R_{rout}^{2np_s+1}(A_{2n}^{(0)}\cos\phi - C_{2n}^{(0)}\sin\phi)}{R_{rout}^{2np_s+2} - R_s^{2np_s+2}} \quad (B.14)$$

$$G_{2n}^{(1)} = -\frac{np_s R_{rout}^{2np_s+1}(A_{2n}^{(0)}\sin\phi + C_{2n}^{(0)}\cos\phi)}{R_{rout}^{2np_s+2} - R_s^{2np_s+2}} \quad (B.15)$$

$$H_{2n}^{(1)} = -\frac{np_s R_s^{2np_s+2} R_{rout}^{2np_s+1}(A_{2n}^{(0)}\sin\phi + C_{2n}^{(0)}\cos\phi)}{R_{rout}^{2np_s+2} - R_s^{2np_s+2}} \quad (B.16)$$

$$S_{2n}^{(1)} = \frac{-\frac{1}{4}anp_s R_{rout}^{2np_s-3}(A_{2n}^{(0)}\cos 2\phi + C_{2n}^{(0)}\sin 2\phi)}{R_{rout}^{2np_s-4} - R_s^{2np_s-4}} \quad (B.17)$$

$$T_{2n}^{(1)} = \frac{-\frac{1}{4}anp_s R_s^{2np_s-4} R_{rout}^{2np_s-3}(A_{2n}^{(0)}\cos 2\phi + C_{2n}^{(0)}\sin 2\phi)}{R_{rout}^{2np_s-4} - R_s^{2np_s-4}} \quad (B.18)$$

$$U_{2n}^{(1)} = \frac{-\frac{1}{4}anp_s R_{rout}^{2np_s-3}(-A_{2n}^{(0)}\sin 2\phi + C_{2n}^{(0)}\cos 2\phi)}{R_{rout}^{2np_s-4} - R_s^{2np_s-4}} \tag{B.19}$$

$$V_{2n}^{(1)} = \frac{-\frac{1}{4}anp_s R_s^{2np_s-4} R_{rout}^{2np_s-3}(-A_{2n}^{(0)}\sin 2\phi + C_{2n}^{(0)}\cos 2\phi)}{R_{rout}^{2np_s-4} - R_s^{2np_s-4}} \tag{B.20}$$

$$W_{2n}^{(1)} = \frac{-\frac{1}{4}anp_s R_{rout}^{2np_s+1}(A_{2n}^{(0)}\cos 2\phi - C_{2n}^{(0)}\sin 2\phi)}{R_{rout}^{2np_s+4} - R_s^{2np_s+4}} \tag{B.21}$$

$$X_{2n}^{(1)} = \frac{-\frac{1}{4}anp_s R_s^{2np_s+4} R_{rout}^{2np_s+1}(A_{2n}^{(0)}\cos 2\phi - C_{2n}^{(0)}\sin 2\phi)}{R_{rout}^{2np_s+4} - R_s^{2np_s+4}} \tag{B.22}$$

$$Y_{2n}^{(1)} = \frac{-\frac{1}{4}anp_s R_{rout}^{2np_s+1}(A_{2n}^{(0)}\sin 2\phi + C_{2n}^{(0)}\cos 2\phi)}{R_{rout}^{2np_s+4} - R_s^{2np_s+4}} \tag{B.23}$$

$$Z_{2n}^{(1)} = \frac{-\frac{1}{4}anp_s R_s^{2np_s+4} R_{rout}^{2np_s+1}(A_{2n}^{(0)}\sin 2\phi + C_{2n}^{(0)}\cos 2\phi)}{R_{rout}^{2np_s+4} - R_s^{2np_s+4}} \tag{B.24}$$

REFERENCES

[1] K. Atallah and D. Howe, "A novel high-performance magnetic gear," *IEEE Trans. Magn.*, vol. 37, no. 4, pp. 2844–2846, Jul. 2001.

[2] L. Jing, Z. Huang, J. Chen, and R. Qu, "An asymmetric pole coaxial magnetic gear with unequal Halbach arrays and spoke structure," *IEEE Trans. Appl. Supercond.*, vol. 30, no. 4, Jun. 2020, Art. no. 5200305.

[3] J. Rens, R. Clark, S. Calverley, K. Atallah, and D. Howe, "Design, analysis and realization of a novel magnetic harmonic gear," in *Proc. 18th Int. Conf. Electr. Mach.*, Vilamoura, Portugal, Sep. 2008, pp. 1–4.

[4] L. Jing, J. Gong, J. Chen, Z. Huang, and R. Qu, "A novel coaxial magnetic gear with unequal Halbach arrays and non-uniform air gap," *IEEE Trans. Appl. Supercond.*, vol. 30, no. 4, Jun. 2020, Art. no. 5000105.

[5] P. Jalali, S. Taghipour Boroujeni, and N. Bianchi, "Simple and efficient model for slotless eccentric surface-mounted PM machines," *IET Electr. Power Appl.*, vol. 11, no. 4, pp. 631–639, Apr. 2017.

[6] L. Jing, J. Cheng, and T. Ben, "Analytical method for magnetic field and electromagnetic performances in switched reluctance machines," *J. Electr. Eng. Technol.*, vol. 14, no. 4, pp. 1625–1635, Jul. 2019.

[7] J. Fu and C. Zhu, "Subdomain model for predicting magnetic field in slotted surface mounted permanent-magnet machines with rotor eccentricity," *IEEE Trans. Magn.*, vol. 48, no. 5, pp. 1906–1917, May 2012.

[8] M. Desvaux, S. Sire, S. Hlioui, H. Ben Ahmed, and B. Multon, "Development of a hybrid analytical model for a fast computation of magnetic losses and optimization of coaxial magnetic gears," *IEEE Trans. Energy Convers.*, vol. 34, no. 1, pp. 25–35, Mar. 2019.

[9] A. Rahideh and T. Korakianitis, "Analytical open-circuit magnetic field distribution of slotless brushless permanent-magnet machines with rotor eccentricity," *IEEE Trans. Magn.*, vol. 47, no. 12, pp. 4791–4808, Dec. 2011.

[10] U. Kim and D. K. Lieu, "Magnetic field calculation in permanent magnet motors with rotor eccentricity: Without slotting effect," *IEEE Trans. Magn.*, vol. 34, no. 4, pp. 2243–2252, Jul. 1998.

[11] U. Kim and D. K. Lieu, "Magnetic field calculation in permanent magnet motors with rotor eccentricity: With slotting effect considered," *IEEE Trans. Magn.*, vol. 34, no. 4, pp. 2253–2266, Jul. 1998.

[12] T. Lubin, S. Mezani, and A. Rezzoug, "Analytical computation of the magnetic field distribution in a magnetic gear," *IEEE Trans. Magn.*, vol. 46, no. 7, pp. 2611–2621, Jul. 2010.

[13] L. Jing, L. Liu, M. Xiong, and D. Feng, "Parameters analysis and optimization design for a concentric magnetic gear based on sinusoidal magnetizations," *IEEE Trans. Appl. Supercond.*, vol. 24, no. 5, Oct. 2014, Art. no. 0600905.

[14] L.-B. Jing, Z.-H. Luo, L. Liu, and Q.-X. Gao, "Optimization design of magnetic gear based on genetic algorithm toolbox of MATLAB," *J. Electr. Eng. Technol.*, vol. 11, no. 5, pp. 1202–1209, Sep. 2016.

[15] Y. Zhang, J. Zhang, and R. Liu, "Magnetic field analytical model for magnetic harmonic gears using the fractional linear transformation method," *Chin. J. Electr. Eng.*, vol. 5, no. 1, pp. 47–52, Mar. 2019.

[16] D. Zarko, D. Ban, and T. A. Lipo, "Analytical calculation of magnetic field distribution in the slotted air gap of a surface permanent-magnet motor using complex relative air-gap permeance," *IEEE Trans. Magn.*, vol. 42, no. 7, pp. 1828–1837, Jul. 2006.

[17] S. T. Boroujeni, S. P. Emami, and P. Jalali, "Analytical modeling of eccentric PM-inset machines with a slotless armature," *IEEE Trans. Energy Convers.*, vol. 34, no. 3, pp. 1466–1474, Sep. 2019.

[18] W. B. Fu, H. Huan, and Z. K. Chen, "Mode analyses of quasi-rectangular waveguides by using PMOBG," *J. Jishou Univ.*, vol. 24, no. 4, pp. 43–47, Aug. 2003.

[19] J. D. Cole, and L. E. Levine, *Perturbation Methods in Applied Mathematics*. New York, NY, USA: Springer-Verlag, 1981.

LIBING JING (Member, IEEE) was born in Henan, China, in 1982. He received the B.E. degree from the Zhongyuan University of Technology, Zhengzhou, China, in 2006, and the Ph.D. degree in power electronics and power drive from Shanghai University, in 2013. From October 2016 to November 2018, he worked as a Postdoctoral Student with the Huazhong University of Science and Technology, Wuhan, China. Since July 2016, he has been an Associate Professor with the College of Electrical Engineering and New Energy, China Three Gorges University.

His research activities are related to design, modeling, and analysis of electrical machines.

JUN GONG was born in Hubei, China, in 1993. He received the B.E. degree in electrical engineering and automation from China Three Gorges University, Yichang, China, in 2016, where he is currently pursuing the M.S. degree with the College of Electrical Engineering and New Energy.

His research interests are electromagnetic field analysis design of motor and magnetic gear.

TONG BEN was born in Hebei, China, in 1991. She received the B.E. and Ph.D. degrees in electrical engineering from the Hebei University of Technology, Tianjin, China, in 2013 and 2018, respectively. Since October 2018, she has been a Lecturer with the College of Electrical Engineering and New Energy, China Three Gorges University.

Her research interest includes the stress and vibration analysis of motor cores considering magnetostriction and Maxwell electromagnetic stress.